JCI insight

RESEARCH ARTICLE

Human defects in STAT3 promote oral mucosal fungal and bacterial dysbiosis

Loreto Abusleme,[1,2] Patricia I. Diaz,[3] Alexandra F. Freeman,[4] Teresa Greenwell-Wild,[1] Laurie Brenchley,[1] Jigar V. Desai,[5] Weng-Ian Ng,[6] Steven M. Holland,[4] Michail S. Lionakis,[5] Julia A. Segre,[6] Heidi H. Kong,[7] and Niki M. Moutsopoulos[1]

[1]Oral Immunity and Inflammation Unit, NIDCR, NIH, Bethesda, Maryland, USA. [2]Faculty of Dentistry, University of Chile, Santiago, Chile.[3]Division of Periodontology, Department of Oral Health and Diagnostic Sciences, UConn Health Center, Farmington, Connecticut, USA. [4]Laboratory of Clinical Immunology and Microbiology (LCIM), [5]Fungal Pathogenesis Section, NIAID, [6]Microbial Genomics Section, NHGRI, and [7]Cutaneous Microbiome and Inflammation Section, NIAMS, NIH, Bethesda, Maryland, USA.

Studies in patients with genetic defects can provide unique insights regarding the role of specific genes and pathways in humans. Patients with defects in the Th17/IL-17 axis, such as patients harboring loss-of-function *STAT3* mutations (autosomal-dominant hyper IgE syndrome; AD-HIES) present with recurrent oral fungal infections. Our studies aimed to comprehensively evaluate consequences of *STAT3* deficiency on the oral commensal microbiome. We characterized fungal and bacterial communities in AD-HIES in the presence and absence of oral fungal infection compared with healthy volunteers. Analyses of oral mucosal fungal communities in AD-HIES revealed severe dysbiosis with dominance of *Candida albicans* (*C. albicans*) in actively infected patients and minimal representation of health-associated fungi and/or opportunists. Bacterial communities also displayed dysbiosis in AD-HIES, particularly in the setting of active *Candida* infection. Active candidiasis was associated with decreased microbial diversity and enrichment of the streptococci *Streptococcus oralis* (*S. oralis*) and *S. mutans*, suggesting an interkingdom interaction of *C. albicans* with oral streptococci. Increased abundance of *S. mutans* was consistent with susceptibility to dental caries in AD-HIES. Collectively, our findings illustrate a critical role for STAT3/Th17 in the containment of *C. albicans* as a commensal organism and an overall contribution in the establishment of fungal and bacterial oral commensal communities.

Introduction

Studies in patients with primary immunodeficiencies (PIDs) have uncovered roles of specific genes and pathways in human immunity (1, 2). In this regard, patients with PIDs that present with mucocutaneous infections demonstrate essential pathways for immune-protection at barrier sites. Barrier immune surveillance is of particular significance, as these surfaces are constantly exposed to normal commensal microbiota and pathogens (3). Thus, perturbations in barrier immunity may disrupt the physiologic interplay between commensals and host, altering the composition of commensal microbial communities and often leading to infection susceptibility or microbial dysbiosis-associated immunopathology (4, 5).

Barrier surfaces are equipped with tissue-specific protective immune mechanisms largely dedicated to the maintenance of host-microbial homeostasis (6, 7). While there is significant understanding of the immunological systems of barrier compartments such as the lower gastrointestinal (GI) tract and skin, host-microbiome interactions at the oral mucosa are much less explored. However, the oral mucosa is second only to the lower GI tract as a home to a rich and diverse community of commensal microbes (8) and is the first site of microbial encounter for the immune system in the GI tract. Consequently, host-microbial interactions at this interface are important to define (9, 10).

An immunological mechanism of importance for oral mucosal barrier surveillance is that of Th17- and IL-17 cytokine–mediated immunity. Indeed, patients and mice with defects in Th17/IL-17 immunity have been documented to have severe susceptibility to oral fungal infections (11–15). IL-17–secreting cells (including Th17 cells) have been shown to play a primary role in maintenance of barrier integrity, as well as in host defense, particularly against extracellular bacteria and fungi (16–19). At the oral mucosa, Th17 and other IL-17–producing

Conflict of interest: The authors have declared that no conflict of interest exists.

Submitted: May 9, 2018
Accepted: July 10, 2018
Published: September 6, 2018

Reference information:
JCI Insight. 2018;3(17):e122061.
https://doi.org/10.1172/jci.insight.122061.

Table 1. Demographic and Clinical Information for the AD-HIES cohort

Subjects analyzed (*n*)	36
Age, mean (SD)	34.6 (11.9)
Sex, (female/male)	(24:12)
Race, *n* (%)	
European descent	30 (83.3%)
African American	2 (5.5%)
Other	4 (11.1%)
History of recurrent oral candidiasis	33 (86%)
History of recurrent oral ulcers	13 (36.1%)
Severe dental caries	13 (36.1%)
Xerostomia	7 (19.4%)

cells have been shown to mediate antifungal immunity through secretion of their signature cytokine, IL-17, which stimulates the production of antimicrobial peptides by epithelial cells (20, 21). Among the recognized PIDs with Th17 defects are patients with autosomal-dominant hyper-IgE syndrome (AD-HIES or Job's syndrome), which harbor loss-of-function (LOF) mutations in the *STAT3* gene (22, 23). AD-HIES patients have been classically characterized by the triad of eczema, skin, and lung infections, as well as extremely elevated serum IgE (24, 25). They also present with recurrent oral *Candida* infections, indicating a critical role for STAT3-mediated oral immunity (26, 27). STAT3 is a key transcription factor downstream of cytokine signaling from IL-6, IL-21, IL-10, and IL-23, among other immune mediators. STAT3 is also defined as a key transcription factor in the differentiation of Th17 (28, 29). Oral mucosal candidiasis in AD-HIES has been thought to be due to defective Th17 differentiation and decreased production of select antimicrobial peptides (30–32).

However, although IL-17/Th17–related defects have a dominant oral phenotype, it is not well understood whether defects in STAT3 and related Th17/IL-17 in humans affect commensal microbiome colonization and predispose to mucosal microbial dysbiosis. Interestingly, emerging literature in animal models has linked blockade of IL-17 with defective anti-microbial surveillance and mucosal dysbiosis-associated immunopathology (16, 33, 34).

Therefore, our current study aims to further our understanding of the consequences of LOF *STAT3* and related Th17 defects on establishment and dynamics of the mucosal mycobiome and bacteriome.

Results

LOF STAT3 mutations in humans are linked to recurrent oral candidiasis. To examine the consequences of LOF *STAT3* on oral commensal fungal and bacterial communities, we recruited a large cohort of AD-HIES patients for clinical evaluation and research studies. AD-HIES diagnosis was based on clinical phenotype and confirmed by detection of LOF mutations in the *STAT3* gene. We clinically examined our entire AD-HIES cohort (n = 36) for oral manifestations and obtained detailed medical and dental histories. We documented a significant rate of oral candidiasis, with 86% of the patients reporting recurrent episodes of oral thrush (Table 1). Most patients received antibiotic and antifungal prophylaxis. However, patients reported recurrent oral candidiasis at diagnosis, prior to commencement of antibiotic regimens. Oral mucosal fungal infections in AD-HIES have been previously linked to defects in the differentiation of Th17 cells and to reduced production of antimicrobial peptides human β-defensin 2 and several histatins (32). Consistent with decreased production of antimicrobial peptides, we detected reduced levels of S100A9 levels (a cation-binding protein, usually found as calprotectin) in oral mucosal secretions (saliva) of AD-HIES patients, compared with age- and sex-matched healthy volunteers (Supplemental Figure 1A; supplemental material available online with this article; https://doi.org/10.1172/jci.insight.122061DS1).

Clinical examination revealed active fungal lesions at the time of evaluation in a subset of patients, primarily presenting on the tongue dorsum and buccal mucosal areas (Supplemental Figure 1, B and C). Other significant intraoral findings included recurrent oral ulcers and severe dental caries in 36.1% and xerostomia in 19.4 % of patients (Table 1).

STAT3-mediated immunity is essential for commensalism of Candida albicans (C. albicans). We first set out to evaluate consequences of defective STAT3-mediated mucosal immunity on the oral mycobiome. For these studies, we subsampled a cohort of AD-HIES patients from our population to obtain balanced groups of patients with the presence/absence of active fungal infection for comparison (n = 18, 9 with active lesions [actively infected] and 9 without mucosal lesions [uninfected]), along with age- and sex-matched healthy controls (Supplemental Table 1). We obtained swab samples from AD-HIES patients and healthy controls at distinct mucosal sites where *Candida* infection typically occurs (the tongue dorsum and buccal mucosa).

All samples were subjected to internal transcribed spacer 1 (ITS1) sequencing for characterization of fungal communities. We found distinct mycobiome communities in AD-HIES patients compared with healthy controls (Figure 1A and Supplemental Figure 2A). Actively infected AD-HIES samples

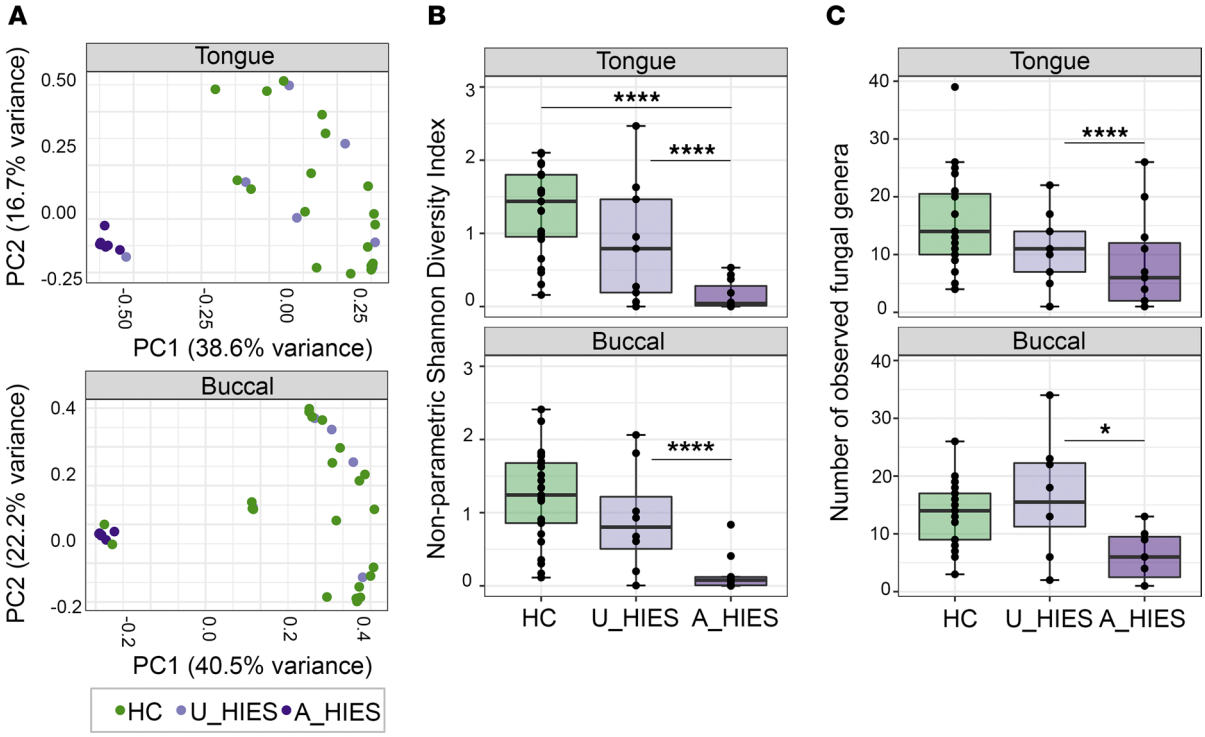

Figure 1. Oral mucosal mycobiome in AD-HIES differs significantly from healthy controls. (**A**) Principal coordinates analysis (PCoA) plot analyzing community structure (based on θ YC distances), showing that fungal communities of patients with autosomal dominant hyper-IgE syndrome (AD-HIES) cluster apart from healthy controls (HC) in tongue and buccal surfaces. $P < 0.001$ as determined by AMOVA comparing HC versus all AD-HIES combined. $P < 0.001$ as determined by AMOVA comparing actively infected (A_HIES, dark purple) and uninfected (U_HIES, light purple) AD-HIES patients. Each circle represents 1 sample. Some data points are not visible, as they get superimposed due to tight clustering. (**B**) Nonparametric Shannon diversity index of tongue and buccal fungal communities of HC, U_HIES, and A_HIES patient samples. ****$P < 0.0001$ as determined by Kruskall-Wallis test and Dunn's multiple comparisons test. (**C**) Number of observed fungal genera in tongue and buccal communities of HC, U_HIES, and A_HIES patient samples. ****$P < 0.0001$ and *$P < 0.01$ as determined by Kruskall-Wallis test and Dunn's multiple comparisons test. (**A–C**) The number of samples per group included in these graphs for HC were $n = 23$ for tongue and $n = 25$ for buccal, and $n = 9$ for tongue and $n = 8$ for buccal for both U_HIES and A_HIES patient groups. Boxes extend from the 25th to 75th percentiles, and the whiskers were plotted from the minimum to maximum value. All outlying values were shown.

also significantly separated from uninfected patients, based on measures of community structure (θ YC distances) and membership (Jaccard index) both in tongue and buccal sites (Figure 1A and Supplemental Figure 2A). Evaluation of diversity of fungal communities based on the Shannon diversity index and the examination of the number of observed fungal genera revealed a decrease in fungal diversity in the actively infected AD-HIES patients (Figure 1, B and C).

Fungal communities from actively infected AD-HIES patients were dominated by the genus *Candida*, accounting for 87.1%–100% abundance on tongue and 85%–100% on buccal lesions (Figure 2A). Species-level classification of *Candida* sequences revealed *C. albicans* as the most abundant taxa in actively infected AD-HIES communities, displaying 84.2%–100% of relative abundance in tongue samples and 57.6 %–100% in buccal samples (Figure 2A and Supplemental Figure 3), suggesting that oral candidiasis in AD-HIES represents a specific overgrowth of *C. albicans*. Consistent with this, *C. albicans* quantitation by real-time PCR was 2 logs higher in actively infected patients than in healthy controls or uninfected patients (Figure 2B). AD-HIES individuals did not harbor unique fungal taxa compared with healthy controls. Interestingly, antifungal treatment did not appear to alter mycobiome communities. Approximately half of *Candida*-infected and half of the uninfected patients were receiving antifungal regimens (Supplemental Table 1), yet the structure and composition of mycobiome communities did not significantly differ based on antifungal therapy (Supplemental Figure 4).

Fungal communities from uninfected AD-HIES patients were dominated by the genus *Malassezia* with representation of *C. dubliniensis* (Figure 2). Highlighting the commensal nature of *C. albicans* and the specificity of its opportunism in AD-HIES is the observation that the mycobiomes of a small number of healthy individuals and 1 uninfected AD-HIES patient were also dominated by *C. albicans* (Figure 2), despite absence of active *Candida* infection and despite the fact that *C. albicans* was detected by real-time PCR in healthy volunteers.

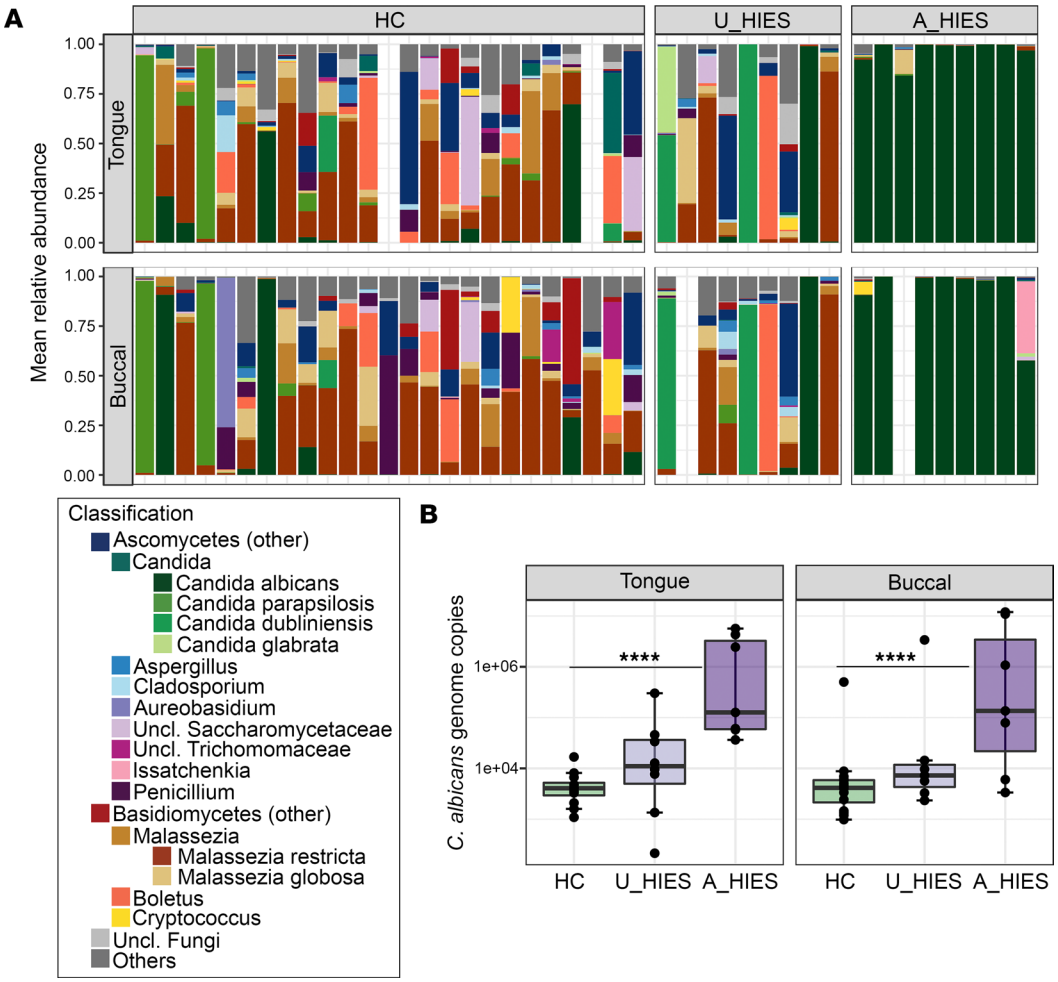

Figure 2. Actively infected AD-HIES oral mucosal fungal communities are dominated by *Candida albicans*. (**A**) Relative abundance plot depicts the major fungal taxa across communities in healthy controls (HC) and patients with AD-HIES. Patient groups shown are HC (n = 23 for tongue, n = 25 for buccal), uninfected AD-HIES (U_HIES, n = 9 for tongue and n = 8 for buccal), and actively infected HIES (A_HIES, n = 9 for tongue and n = 8 for buccal). *Malassezia* and *Candida* genera were further classified to species level due to abundance and clinical relevance. Each bar represents 1 subject. Empty bars represent missing samples. (**B**) *Candida albicans* genome copies per μg of DNA in tongue and buccal fungal communities from HC (n = 12 for tongue and n = 16 for buccal), uninfected (U_HIES, n = 8 for tongue and n = 7 for buccal), and actively infected (A_HIES, n = 7 for tongue and n = 7 for buccal) AD-HIES patients, quantified by real-time PCR. *Candida albicans* biomass values are expressed as $\log_{10}$ of genome copies. ****$P < 0.0001$ as determined by Kruskall-Wallis test and Dunn's multiple comparisons test. Boxes extend from the 25th to 75th percentiles, and the whiskers were plotted from the minimum to maximum value. All outlying values were shown.

Our evaluation also afforded a detailed view of the oral mycobiome in 2 distinct oral mucosal surfaces in healthy subjects (Figure 2A). We observed high variability in fungal composition of mycobiome communities in healthy controls, with a predominance of the genus *Malassezia* in both tongue and buccal surfaces. Within the *Candida* genus, *C. albicans* was the most common species observed in health-associated communities. *C. parapsilosis*, *Boletus*, and *Penicillium* were also among the highly abundant fungal taxa present in communities from healthy controls.

Collectively, our characterization of fungal communities in AD-HIES and healthy controls demonstrates that oral mucosal fungal infections in AD-HIES are dominated by the opportunistic yeast *C. albicans*, revealing a specific role for STAT3/Th17-mediated immunity in containing *C. albicans* as a commensal organism.

Defects in STAT3-mediated immunity are associated with shifts in bacterial communities. We next aimed to characterize the consequences of STAT3 deficiency on oral mucosal bacterial communities. For this, we performed 16S rRNA gene sequencing on the identical samples analyzed for mycobiome. Evaluating samples from *Candida*-infected and uninfected AD-HIES individuals allowed us to characterize the consequences of STAT3 deficiency on the oral microbiome alone and in the presence of active candidiasis. We found that bacterial communities in AD-HIES separated from those of healthy controls based on measures

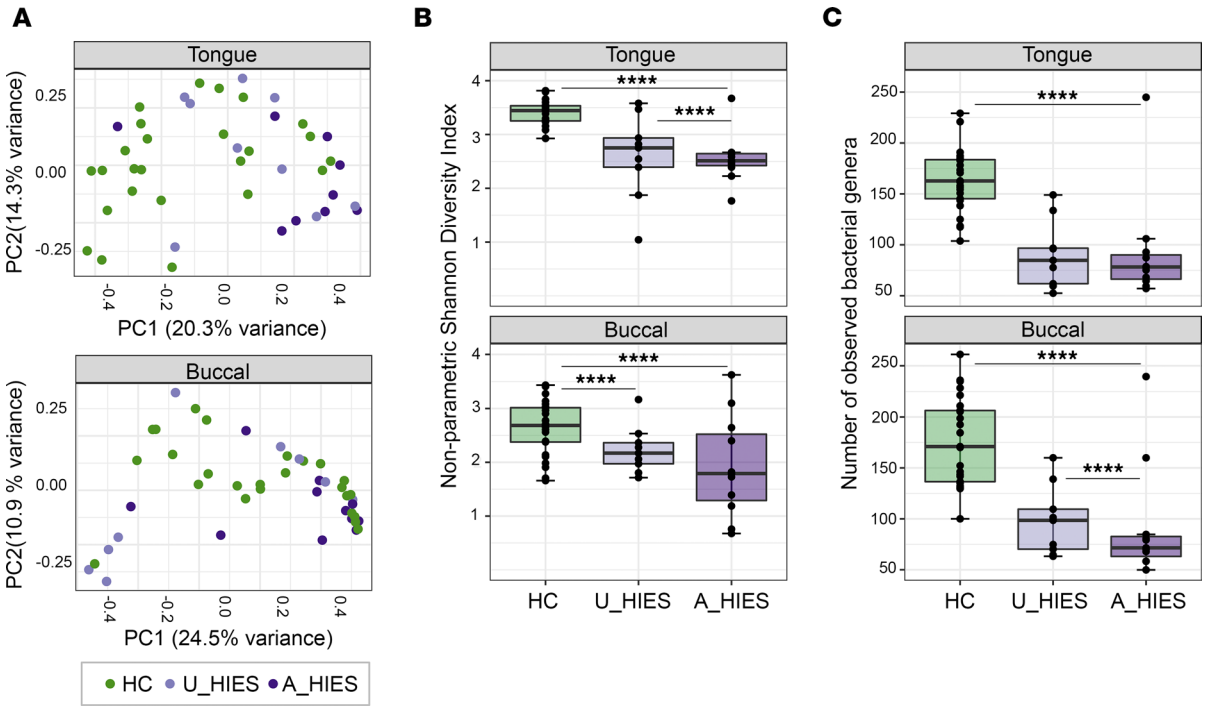

Figure 3. AD-HIES oral mucosal bacterial communities differ significantly from healthy controls. (**A**) Principal coordinates analysis (PCoA) plot analyzing community structure (based on θ YC distances) of the bacterial microbiome in HC and AD-HIES. For the tongue plot, $P < 0.001$ comparing HC vs. all AD-HIES combined and $P = 0.103$ (ns) comparing actively infected HIES (A_HIES) and uninfected HIES (U_HIES) samples as determined by AMOVA. For buccal plot, $P < 0.05$ comparing HC vs. all HIES combined and $P = 0.118$ (ns) comparing A_HIES versus U_HIES, as determined by AMOVA. Each circle represents 1 sample. (**B**) Nonparametric Shannon diversity index of tongue and buccal bacterial communities of HC and AD-HIES patients. ****$P < 0.0001$ as determined by Kruskall-Wallis test and Dunn's multiple comparisons test. (**C**) Number of observed bacterial species in tongue and buccal communities of HC and AD-HIES patients. ****$P < 0.0001$ as determined by Kruskall-Wallis test and Dunn's multiple comparisons test. (**A–C**) The number of samples per group included in these graphs for HC were $n = 25$ for tongue and buccal, for U_HIES $n = 9$ for tongue and buccal, and for A_HIES $n = 9$ for tongue and $n = 8$ for buccal. Boxes extend from the 25th to 75th percentiles, and the whiskers were plotted from the minimum to maximum value. All outlying values were shown.

of community structure (θ YC distances) and composition (Jaccard index) (Figure 3A and Supplemental Figure 2B). AD-HIES microbial communities displayed decreased diversity with a reduced number of bacterial species, particularly in the setting of candidiasis (Figure 3, B and C).

We next sought to characterize the composition of bacterial communities in AD-HIES patients compared with healthy controls by evaluating the relative abundance of main bacterial taxa. *Streptococcus*, *Prevotella*, and *Rothia* were the most abundant bacterial constituents across all samples (Figure 4). Evaluation of bacterial taxa present in AD-HIES compared with healthy controls revealed several bacterial taxa differentially abundant between groups. Several common oral commensal bacterial species and genera — including *Neisseria*, *Porphyromonas*, and *Haemophilus* — had a significantly lower relative abundance in AD-HIES, while the genus *Capnocytophaga* and TM7 [G-1] were overrepresented in either tongue or buccal AD-HIES samples (Supplemental Figure 5).

Candida infection in AD-HIES patients is associated with increased abundance of streptococci and increased dental caries. To specifically assess the effect of *Candida* infection on the oral mucosal microbiome in the setting of AD-HIES, we next interrogated differences in bacterial genera in infected compared with uninfected patients. Our key finding was the increase in relative abundance of the genus *Streptococcus* in actively infected patients. Microbial communities from infected AD-HIES patients displayed an increase in the relative abundance of the *Streptococcus* genus (Figure 4), and linear discriminant analysis effect size (LEfSe) analysis revealed a significantly increased relative abundance of *Streptococcus* in both tongue and buccal mucosa of candidiasis-infected AD-HIES patients (Figure 5A). *Streptococcus* biomass was also greater in buccal mucosa of *Candida*-infected AD-HIES patients compared with healthy controls (Figure 5B). Interestingly, investigating the bacterial species overrepresented in buccal samples from *Candida*-infected AD-HIES sites, we found increased abundance specifically of *Streptococcus mutans* (*S. mutans*) and *Streptococcus oralis* (*S. oralis*) (Figure 5C).

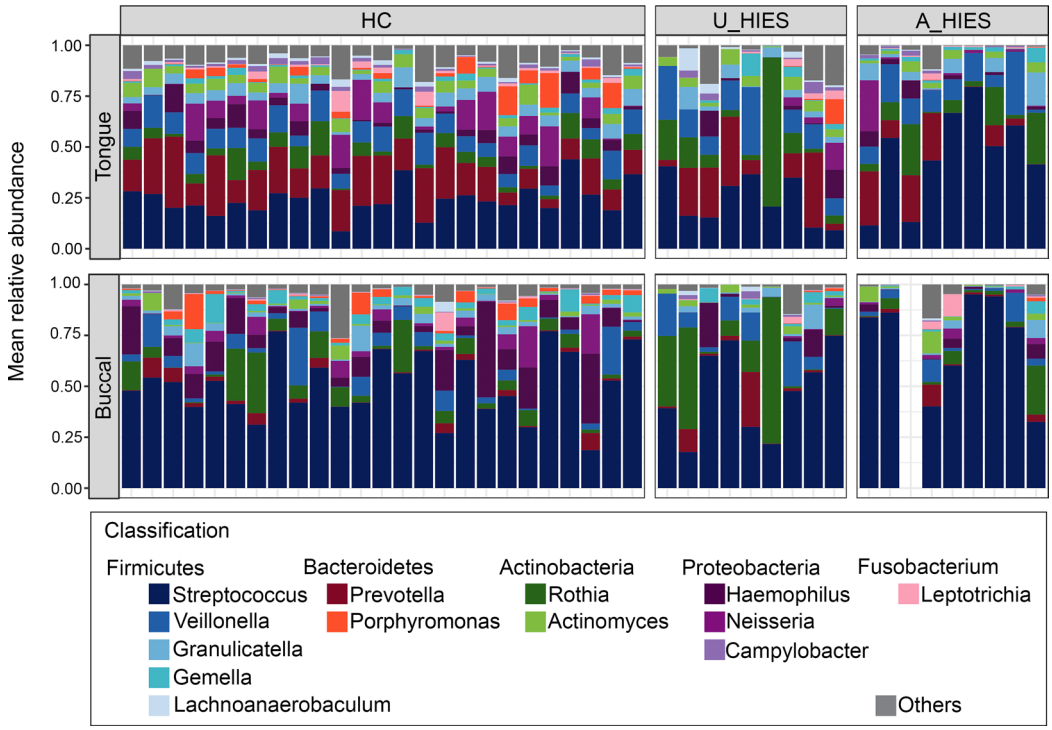

Figure 4. Overview of most abundant bacterial genera in oral mucosal microbiome of AD-HIES compared with HC. Relative abundance plots depict the major bacterial genera in tongue and buccal samples from HC, actively infected (A_HIES), and uninfected (U_HIES) patients with AD-HIES. Each bar represents 1 subject. Empty bar represents a missing sample.

Exploring the possible functional consequences of overgrowth of select *Streptococcus spp*. in the oral microbiome of AD-HIES patients, we evaluated the presence and severity of streptococci-associated oral infections in AD-HIES patients. *S. mutans* is recognized as the main etiologic agent of dental caries and was detected with increased relative abundance in candidiasis-affected AD-HIES patients. Interestingly, our original clinical examination had indicated high rates of dental infections in AD-HIES (Table 1).

Therefore, we quantitatively assessed dental caries in AD-HIES patients compared with age- and sex-matched healthy volunteers (AD-HIES $n = 36$, healthy controls $n = 22$). The prevalence of caries was evaluated by assessment of missing, decayed, and filled teeth (DFMT) on dental radiographs from AD-HIES and healthy controls. We found a significant increase in the prevalence of dental caries in the AD-HIES cohort (Figure 5D).

While a causative relationship between *Candida* infection, streptococcal overgrowth, and dental infections cannot be conclusively established based on our cross-sectional study, our data suggest that immune defects in AD-HIES are associated with *C. albicans* infection and microbial dysbiosis linked to streptococcal overgrowth.

Discussion

Studies in experimental models and humans with defects in IL-17/Th17 have suggested that the Th17 pathway is critical in the surveillance of *C. albicans* (11, 20, 33, 34). Defects of Th17 differentiation have been previously documented in patients with LOF mutations of STAT3 (30, 31) and linked to oral candidiasis (26, 27). However, the consequences of defective STAT3/Th17-mediated immunity have not been thoroughly evaluated at the oral mucosal barrier in humans. Our work aimed to further our understanding of STAT3/Th17-mediated mucosal immunity in humans and its consequences on the oral mucosal mycobiome and bacteriome. Toward this goal, we recruited a large cohort of patients with LOF mutations in *STAT3* (AD-HIES, $n = 36$) and performed clinical, immunological, and microbiome studies at the oral mucosal barrier. Clinical phenotyping of our cohort of AD-HIES patients confirmed previous reports of increased rates of oral candidiasis (26, 27), revealing recurrent candidiasis in 86% of the population. Predominant sites affected by candidiasis were the buccal mucosa and dorsum of tongue. We sampled a subset of our population to include 50% of patients with active oral candidiasis and allow for a balanced sampling of

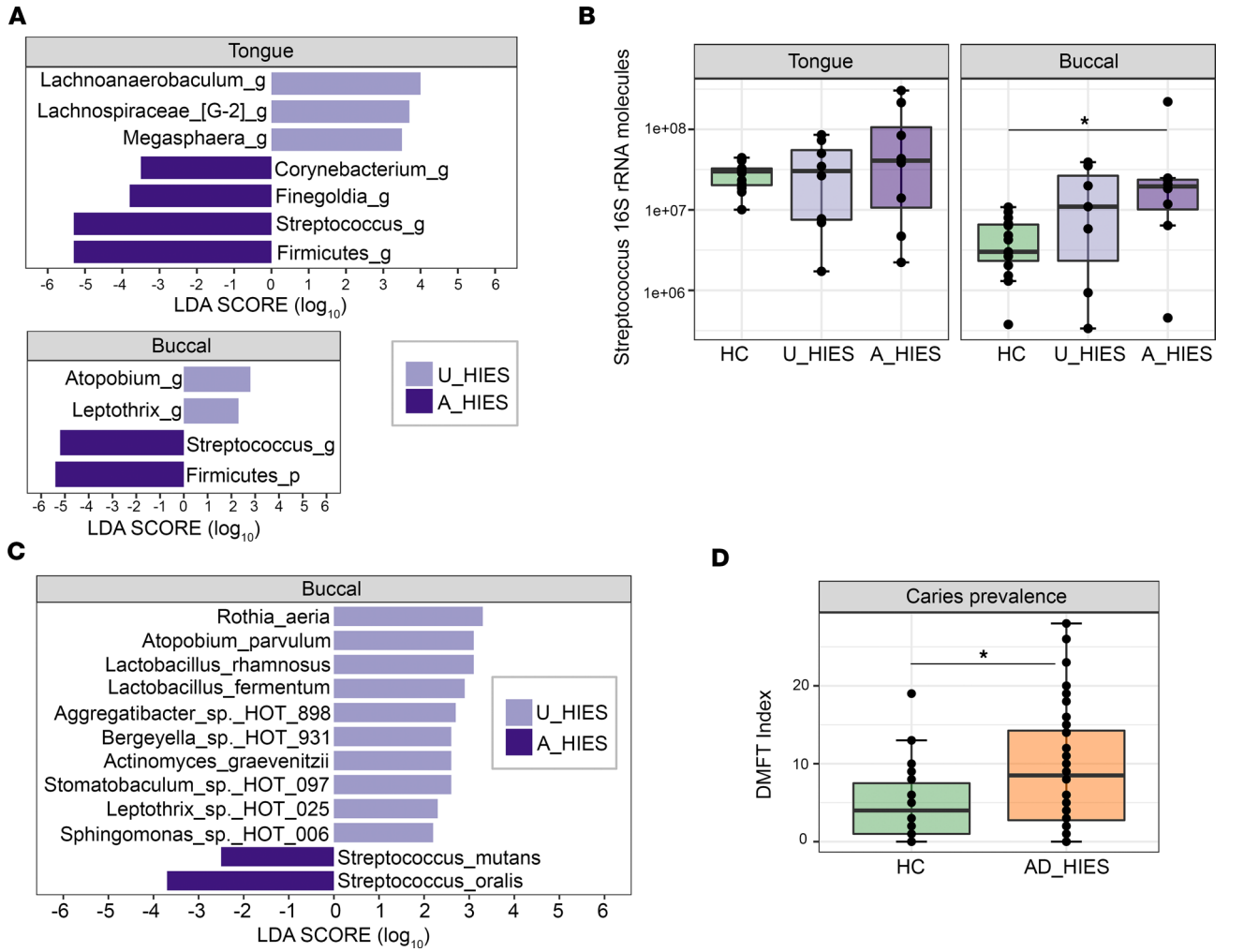

Figure 5. Increase in oral streptococci and dental caries susceptibility in AD-HIES. (**A**) Differentially represented bacterial genera in actively infected (A_HIES, *n* = 9 for tongue and *n* = 8 for buccal samples) and uninfected (U_HIES, *n* = 9 for tongue and buccal samples) patients with AD-HIES, determined via LEfSe analysis. (**B**) Real-time PCR quantitation of the genus *Streptococcus* in tongue and buccal surfaces of HC and AD-HIES patients. The number of samples included in the tongue panel were HC *n* = 15, U_HIES *n* = 8, and A_HIES *n* = 8; for the buccal panel, number of samples were HC *n* = 15, U_HIES *n* = 7, and A_HIES *n* = 8. *Streptococcus* biomass values are expressed as $\log_{10}$ of 16S rRNA gene copy number. **P* < 0.02 as determined by Kruskall-Wallis test and Dunn's multiple comparisons test. (**C**) Differentially represented bacterial species found in actively infected and uninfected AD-HIES buccal samples, determined via LEfSe analyses. (**D**) Caries prevalence comparing HC (*n* = 22) and AD-HIES (*n* = 36) calculated using the Decayed, Missing, Filled Teeth (DMFT) index in dental radiographs. **P* < 0.03 as determined by Mann-Whitney *U* test. (**B** and **D**) Boxes extend from the 25th to 75th percentiles, and the whiskers were plotted from the minimum to maximum value. All outlying values were shown.

actively infected and uninfected patients for our microbiome characterization. Additional clinical oral findings included increased susceptibility to oral ulcers and dental caries (36.1%), as well as xerostomia (19%).

We found that the mycobiome and bacteriome in AD-HIES were distinct from those of age- and sex-matched healthy controls, with a significantly reduced diversity of communities, particularly in the presence of active *Candida* infection. These findings were unlike those in skin fungal communities in AD-HIES patients, which had higher diversity than healthy controls. These differences in oral and cutaneous microbiomes may reflect distinct regulatory pathways for microbial colonization at various epithelial sites (35, 36). Therefore, our work underscores the importance of examining tissue-specific differences in microbiome composition. Furthermore, to our knowledge, our studies provide the first characterization of the mucosal fungal and bacterial communities in AD-HIES.

By performing molecular characterization of fungal communities in AD-HIES, we observed dominance of the commensal species *C. albicans*. This suggested a lack of exogenous infection in AD-HIES. In fact, while *C. albicans* was detected by quantitative PCR (qPCR) in the majority of healthy volunteers, its biomass was much higher in AD-HIES, particularly in the setting of active infection. Our findings support

that *Candida* infection in AD-HIES was not related to chronic antibiotic use. AD-HIES patients reported a history of oral thrush prior to diagnosis and commencement of antibiotic use. In fact, the use of antibiotics does not typically predispose to oral candidiasis, unlike vaginal candidiasis (37, 38). Interestingly, in AD-HIES, antifungal treatment did not alter the composition of fungal communities and did not predispose patients to nonalbicans *Candida* infections (39, 40).

Our study also provides a first characterization of fungal communities in distinct oral mucosal sites in healthy individuals. Previous studies have characterized oral mycobiome in oral rinses and saliva, summating fungal communities from all oral sites (41–43). Importantly, our work in the health-related mycobiome found important differences in the buccal mucosal and tongue fungal communities, as well as extensive intraindividual variability. *Malassezia* was the most common shared predominant taxa in healthy individuals and in both mucosal sites studied, similar to reports from human saliva, nares, and skin (42, 44).

We next specifically evaluated the oral microbiome in AD-HIES patients with and without active *Candida* infection. These analyses aim at characterizing the effects of *STAT3* deficiency alone or in combination with *C. albicans* infection on the oral microbiome. Importantly, the setting of AD-HIES and recurrent *Candida* infections provide a unique disease model to evaluate oral microbiome intracommunity relationships in the context of *C. albicans* infection.

Bacterial communities in AD-HIES had reduced diversity and a markedly decreased abundance and presence of common oral commensal bacteria, particularly in the context of oral candidiasis.

Oral candidiasis in AD-HIES was linked to an increased proportion of *Streptococcus spp.*, as well as an increase in the biomass of streptococci, particularly at buccal mucosal sites. *S. oralis* and *S. mutans* were overrepresented on the buccal mucosa in active candidiasis. Previous findings had also demonstrated that oral communities dominated by *Candida* had decreased bacterial richness and increased oral streptococci and other acidophilic taxa (45, 46). Based on the increased representation and biomass of *Streptococcus* in candidiasis in AD-HIES, we suspect a synergistic relationship between *C. albicans* and oral streptococci (47–50). Previous in vitro data has suggested that select oral streptococci enhance *C. albicans* virulence by increasing its capacity to invade oral tissues (47), permitting severe oral thrush lesions in vivo (49). This cooperative relationship may be contributing to candidiasis susceptibility or secondary infections in AD-HIES. The synergy between *C. albicans* and *S. mutans* has been recognized as a key factor in dental caries, due to the metabolism of dietary sugars into glucans and acid, forming a firmly adherent biofilm on the tooth surface, leading to loss of mineralized tissue (50). *C. albicans* amplifies the cariogenic potential of *S. mutans* biofilms by increasing exopolysaccharide production, augmenting biofilm biomass, and enhancing its virulence, which leads to rampant carious lesions in rodent models (48, 51, 52). Indeed, multiple clinical studies have shown that *S. mutans* and *C. albicans* carriage is much higher in early-childhood caries and adults with increased carious lesions compared with caries-free individuals (53–57). Our data further support a cooperative interaction between *C. albicans* and *S. mutans,* as we have documented significantly increased dental caries in AD-HIES patients compared with healthy controls. A small case series had also suggested that AD-HIES patients present with severe carious lesions (58). While our current study has focused on the oral mucosal microbiome, it will be important in future work to evaluate microbiome shifts on the tooth surface where caries occur.

Our work supports a model in which STAT3/Th17 is critical in oral antifungal immunity specifically against *C. albicans*. In the presence of defective STAT3/Th17 immunity, *C. albicans* overgrows and bacterial communities become dysbiotic with a dominance of oral streptococci. Overgrowth of specific oral streptococci may be promoted by *C. albicans* alone and/or facilitated by defective IL-17/Th17 immunity (59, 60), leading to local secondary dental infection caries (Figure 6).

Taken together, our studies in a population of patients with genetic defects in STAT3 reveal a critical role for STAT3-mediated immunity in the oral mucosal surveillance of *C. albicans* and in the establishment of oral commensal fungal and bacterial communities.

Methods

Patient characterization. Diagnosis of autosomal dominant hyper-IgE syndrome was performed using a HIES scoring system that considers the main immunologic/nonimmunologic disease manifestations, as previously described (61) and confirmed by the presence of LOF mutations in the *STAT3* gene. Age- and sex-matched healthy subjects without significant medical histories were included as a healthy-control population. All demographic and relevant medical/dental clinical information was recorded.

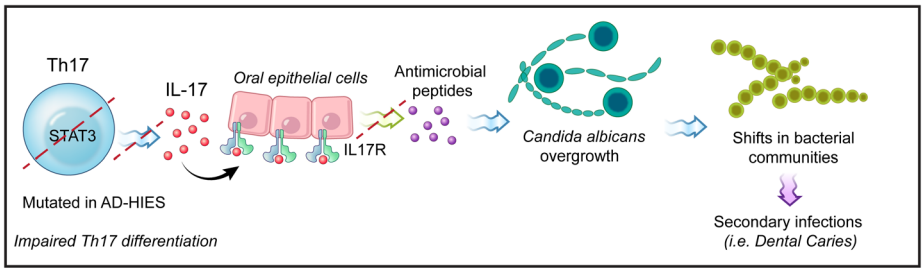

Figure 6. Proposed model in which the STAT3/Th17 axis is critical in oral antifungal immunity specifically against *Candida albicans*. In the presence of defective STAT3/Th17 immunity, *C. albicans* will overgrow and lead to shifts in bacterial communities. Consequent microbial dysbiosis (i.e., increase in specific oral streptococci) may contribute to local secondary infections.

Oral examination and microbiome sample collection. Questionnaires of dental history were completed for all patients. Data related to dental/oral findings including history of recurrent oral thrush, recurrent oral ulcers, xerostomia (subjective reporting combined with minimal or no unstimulated saliva), and severe caries susceptibility (defined as generalized carious lesions or restorations on >30% of dentition) were recorded. All AD-HIES patients and healthy volunteers received an oral examination and a panoramic radiograph. Clinical diagnosis of oral candidiasis in AD-HIES individuals was made upon detection of white lesions that rubbed off with gauze. Caries status determination was performed recording the Decayed, Missing, Filled Teeth (DMFT) index using panoramic radiographs. Patients were given instructions not to eat, not to drink anything other than water, not to chew gum 2 hours before sample collection, and to refrain from oral hygiene for 12 hours before sampling. Samples for oral mucosal microbiome analyses were collected from tongue dorsum and buccal mucosa areas by rubbing for 10 seconds using CatchAll swabs (Epicentre), which were then placed in Yeast Lysis buffer (Epicentre) and stored at –80°C until processing. Patients with xerostomia were excluded from research sampling procedures.

Saliva sample collection and S100A9 ELISA. Unstimulated saliva samples were obtained by expectoration into a polypropylene tube kept on ice for 5 minutes. Saliva samples were centrifuged at 2,600 *g* for 15 minutes; then, the supernatant was recovered and proteinase inhibitors (Roche Diagnostics) were added. Samples were stored at –80°C until processing. S100A9 protein levels were measured using an ELISA-based kit (R&D, catalog DY5578), following the manufacturer's instructions.

DNA isolation, library preparation, and sequencing. DNA was extracted using the protocol previously detailed in Jo et al. (62). Briefly, oral mucosal swab samples were subjected to an enzymatic lysis step that included the addition of ReadyLyse Lysozyme solution (Epicentre) and a 1-hour incubation at 37°C in a shaking thermal block. To mechanically dissociate fungal and bacterial cells walls, 2 steel beads (5 mm, Qiagen) were added to each tube to perform a bead-beating step in a TissueLyser (Qiagen) for 2 minutes at 30 Hz. Then, samples were incubated at 65°C for 30 minutes to finalize lysis, followed by addition of the MPC Reagent (Epicentre), and their processing continued using the PureLink Genomic DNA Kit (Invitrogen) according the manufacturer's instructions. DNA was eluted in 35 μl of PCR grade water (MoBio).

For 16S rRNA gene amplicon sequencing, the V1-V3 region was amplified using the primers V1_27F (5′-CCTATCCCCTGTGTGCCTTGGCAGTCTCAGAGAGTTTGATCCTGGCTCAG-3′) and V3_534R (5′-CAGCACGCATTACCGCGGCTGCTGG-3′) (44). For ITS1 amplicon sequencing, the ITS1 region was amplified using the primers 18SF (5′-CCTATCCCCTGTGTGCCTTGGCAGTCTCAGGTAAAAGTCGTA ACAAGGTTTC-3′) and 5.8S-1R (5′-GTTCAAAGAYTCGATGATTCAC-3′) (44). Both primer pairs (for 16S rRNA V1-V3 and ITS1) included 5′ and 3′ linker sequences, heterogeneity spacers, and index identifiers to allow dual indexing as previously described (63).

The PCR reaction for 16S rRNA and ITS1 amplification were the following: 2.5 μl 10× PCR buffer, 4 μl deoxynucleotide (dNTP) mix, 0.25 μl Taq polymerase (Takara), 1 μl of each Forward and Reverse primer, 2.5 μl of isolated microbial DNA, and 13.75 l of PCR-grade water. The thermal cycling conditions for 16S rRNA gene library amplification included an initial denaturation step of 95°C for 2 minutes and 30 cycles of denaturation at 95°C for 20 seconds, with annealing at 56°C for 30 seconds and extension at 72°C for 60 seconds. The thermal cycling conditions for ITS1 gene library amplification included an initial denaturation step of 95°C for 2 minutes, 30 cycles of denaturation at 95°C for 30 seconds, annealing at 50°C

for 30 seconds, extension at 72°C for 2 minutes, and a final extension at 72°C for 5 minutes. PCR reactions were carried out in duplicate; then, PCR products were combined, purified using Agencourt AMPureXP (Beckman Coulter), and quantified via Quant-IT dsDNA Kit (Invitrogen; Life Technologies). Approximately equivalent amounts of each PCR product were then combined and purified using the MinElute PCR purification kit (Qiagen) and sequenced at the NIH Intramural Sequencing Center on an Illumina MiSeq platform.

16S rRNA gene amplicon sequence analysis pipeline. Reads were processed using the software mothur (64). Preprocessing steps included contig assembly, trimming (primers, spacers, and indices), and size filtering to include sequences with a maximum length of 510 bp and no ambiguous base calls. Sequences were then processed according to an established mothur-based pipeline (65). Chimeric sequences were detected using UCHIME (66) as implemented in mothur and subsequently removed. For taxonomical assignment, we performed a phylotype analysis using the Human Oral Microbiome Database (HOMD) version 14.5 as a reference (67). Reads were classified up to the species level by using the BLAST option and the k-nearest neighbor algorithm within mothur following the parameters established and validated by Al-Hebshi et al. (68).

ITS1 gene amplicon sequence analysis pipeline. Reads were preprocessed and chimeric sequences removed following the same procedures described for the 16S rRNA amplicon data (see above). For taxonomical classification, we used a modified version of a previously generated custom fungal ITS1 reference database (44). Modifications included a revision of fungal nomenclature, with synonym fungal genera collapsed and given a consensus genus name according to the recommendation of Dupuy et al. (42) and current literature. Additionally, sequences belonging to *Aspergillus*/*Emericella* genera were manually curated by eliminating a fraction of them that were misclassified as fungi. With this updated ITS1 database as our reference, sequences were classified down to the genus level by BLAST and the k-nearest neighbor algorithm in mothur using the parameters previously determined and validated by Findley et al. (44).

Candida and *Malassezia* ITS1 reads were further classified to species level following the same procedures previously described for *Malassezia* speciation (44). Briefly, *Candida* sequences were extracted from our dataset through the get.lineage command in mothur. We then constructed a *Candida* ITS1 reference package by retrieving and aligning *Candida* type-strain ITS1 sequences. This manually curated *Candida* ITS1 database was used for phylogenetic classification of *Candida* reads via the pplacer software package (69), considering a likelihood score higher than 0.65.

α- *And* β-*diversity estimates for 16S rRNA and ITS1 data*. Measures of community diversity (nonparametric Shannon index), community structure (θ YC index), and membership (Jaccard index) were calculated using mothur, after subsampling at 25,000 reads per sample for 16S rRNA data and 3,000 reads for ITS1 data. These metrics were constructed based on species-level taxonomic units for 16S rRNA and genus-level for ITS1 (with the exception of *Candida* that was speciated). The lower subsampling cut-off for fungal data was due to the lower amount of sequences recovered in samples from healthy controls. Principal coordinates analyses (PCoA) was performed in mothur.

Quantification of Streptococcus and Candida biomass. Determination of *Streptococcus* load was performed via real-time PCR using 16S rRNA gene-based primers, as previously described (70). The standard curves consisted of genomic DNA of *S. gordonii* (ATCC, 35105), which was serially diluted to obtain a range from 1×10^2 to 1×10^8 16S rRNA gene molecules. PCR reactions were carried out using a final volume of 50 μl; each reaction consisted of 25 μl of SYBR Green PCR Master Mix (Invitrogen; Life Technologies), 500 nM of each primer, 1 μl of DNA from each sample, and PCR water (MoBio). Thermal cycle conditions comprised 95°C for 10 minutes, 40 cycles of 95°C for 15 seconds, and 60°C for 1 minute. A melting curve analysis for *Streptococcus* PCR products was performed and revealed a single sharp peak, confirming the specificity of the assay.

For quantification of *C. albicans* burden, real-time PCR reactions were run using 8 ng of total DNA mixed with 500 nM *C. albicans*–specific primers (that target the SAP5 gene) (71) and PerfecTa SYBR Green Fastmix (Quanta Biosciences). The cycling protocol involved an initial denaturation step at 95°C for 3 minutes, followed by 40 cycles of 95°C for 15 seconds and 60°C for 1 minute. *C. albicans* genome copy values were calculated from a standard curve prepared using DNA isolated from pure *C. albicans* cultures. This quantitation was performed taking into consideration that the *C. albicans* genome harbors a single copy of the SAP5 gene, and since this yeast has a diploid genome, there are 2 copies of the SAP5 gene in 1 CFU equivalent genome, allowing direct extrapolation from CFUs to genome equivalents. Briefly, 9×10^8 blastopores of *C. albicans* were resuspended in 300 μl of sterile TENTS (10mM Tris-HCl, pH 8.0 containing

1mM EDTA, 100mM NaCl, 2% Triton X-100 and 1% SDS; all from MilliporeSigma), and DNA isolation was done as described previously (72).

All real-time assays were performed in a 7500 Real-Time PCR system (Invitrogen; Life Technologies), and PCR reactions were carried out in triplicate.

Data access. All sequence data from this study have been submitted SRA under the to NCBI BioProject 413203 (https://www.ncbi.nlm.nih.gov/bioproject) under accession number 413203.

Statistics. Patient demographic data (age and sex) were compared via unpaired 1-taield *t* test and Fisher's test, respectively. Dissimilarities in α diversity, number of taxa and real-time data among healthy controls, and uninfected and actively infected AD-HIES samples were determined using 1-way ANOVA or Kruskall-Wallis tests according to data distribution. Comparisons for S100A9 levels and DMFT scores between healthy and AD-HIES patients were assessed using Mann-Whitney *U* tests. Analysis of Molecular Variance (AMOVA) was used to test differences for PCoA analyses of community structure and membership. For all of these previously mentioned statistical analysis, a value of $P < 0.05$ was considered significant. For 16S rRNA and ITS1 sequencing data, differences in relative abundance between groups was evaluated using LEfSe (73) considering 0.01 as the α value for statistical testing. All graphs and analyses were generated using R software.

Study approval. All patient-related activities in this study were conducted under IRB approved protocols (NIDCR and NIAID from NIH). All participants provided written informed consent prior to inclusion in the study.

Author contributions

LA and NMM conceived of the study, performed data collection and data analyses, and wrote the manuscript; PID, MSL, JAS, and HHK provided insights in data analysis and data interpretation and edited the manuscript; AFF and SMH supervised the medical team involved in patient care, provided insights in data interpretation, and edited the manuscript; TGW, LB, JVD, and WIN participated in data collection; NMM supervised the study.

Acknowledgments

This work was supported in part by the Intramural Programs of the NIDCR, NHGRI, NIAMS, and NIAID from the NIH. Additionally, authors were funded by extramural grants from NIDCR R01 DE021578 and R21DE023967 (to PID). The authors would like to thank Morgan Park, Sean Conlan, and Xin Huang for their input in data presentation and processing.

Address correspondence to: Niki M. Moutsopoulos, 30 Convent Drive, Bethesda, Maryland 20892, USA. Phone: 301.435.7182; Email: nmoutsop@mail.nih.gov.

1. Moutsopoulos NM, Lionakis MS, Hajishengallis G. Inborn errors in immunity: unique natural models to dissect oral immunity. *J Dent Res*. 2015;94(6):753–758.
2. Parvaneh N, Casanova JL, Notarangelo LD, Conley ME. Primary immunodeficiencies: a rapidly evolving story. *J Allergy Clin Immunol*. 2013;131(2):314–323.
3. Belkaid Y, Harrison OJ. Homeostatic Immunity and the Microbiota. *Immunity*. 2017;46(4):562–576.
4. Cho I, Blaser MJ. The human microbiome: at the interface of health and disease. *Nat Rev Genet*. 2012;13(4):260–270.
5. Belkaid Y, Hand TW. Role of the microbiota in immunity and inflammation. *Cell*. 2014;157(1):121–141.
6. Belkaid Y, Segre JA. Dialogue between skin microbiota and immunity. *Science*. 2014;346(6212):954–959.
7. Peterson LW, Artis D. Intestinal epithelial cells: regulators of barrier function and immune homeostasis. *Nat Rev Immunol*. 2014;14(3):141–153.
8. Human Microbiome Project Consortium. Structure, function and diversity of the healthy human microbiome. *Nature*. 2012;486(7402):207–214.
9. Abusleme L, Moutsopoulos NM. IL-17: overview and role in oral immunity and microbiome. *Oral Dis*. 2017;23(7):854–865.
10. Moutsopoulos NM, Konkel JE. Tissue-Specific Immunity at the Oral Mucosal Barrier. *Trends Immunol*. 2018;39(4):276–287.
11. Ho AW, et al. IL-17RC is required for immune signaling via an extended SEF/IL-17R signaling domain in the cytoplasmic tail. *J Immunol*. 2010;185(2):1063–1070.
12. Puel A, et al. Chronic mucocutaneous candidiasis in humans with inborn errors of interleukin-17 immunity. *Science*. 2011;332(6025):65–68.
13. Boisson B, et al. An ACT1 mutation selectively abolishes interleukin-17 responses in humans with chronic mucocutaneous candidiasis. *Immunity*. 2013;39(4):676–686.
14. Ling Y, et al. Inherited IL-17RC deficiency in patients with chronic mucocutaneous candidiasis. *J Exp Med*. 2015;212(5):619–631.

15. Lionakis MS, Netea MG, Holland SM. Mendelian genetics of human susceptibility to fungal infection. *Cold Spring Harb Perspect Med*. 2014;4(6):a019638.
16. Lee JS, et al. Interleukin-23-Independent IL-17 Production Regulates Intestinal Epithelial Permeability. *Immunity*. 2015;43(4):727–738.
17. Maxwell JR, et al. Differential Roles for Interleukin-23 and Interleukin-17 in Intestinal Immunoregulation. *Immunity*. 2015;43(4):739–750.
18. Liang SC, et al. Interleukin (IL)-22 and IL-17 are coexpressed by Th17 cells and cooperatively enhance expression of antimicrobial peptides. *J Exp Med*. 2006;203(10):2271–2279.
19. Weaver CT, Elson CO, Fouser LA, Kolls JK. The Th17 pathway and inflammatory diseases of the intestines, lungs, and skin. *Annu Rev Pathol*. 2013;8:477–512.
20. Conti HR, et al. Th17 cells and IL-17 receptor signaling are essential for mucosal host defense against oral candidiasis. *J Exp Med*. 2009;206(2):299–311.
21. Trautwein-Weidner K, Gladiator A, Nur S, Diethelm P, LeibundGut-Landmann S. IL-17-mediated antifungal defense in the oral mucosa is independent of neutrophils. *Mucosal Immunol*. 2015;8(2):221–231.
22. Holland SM, et al. STAT3 mutations in the hyper-IgE syndrome. *N Engl J Med*. 2007;357(16):1608–1619.
23. Minegishi Y, et al. Dominant-negative mutations in the DNA-binding domain of STAT3 cause hyper-IgE syndrome. *Nature*. 2007;448(7157):1058–1062.
24. Davis SD, Schaller J, Wedgwood RJ. Job's Syndrome. Recurrent, "cold", staphylococcal abscesses. *Lancet*. 1966;1(7445):1013–1015.
25. Buckley RH, Wray BB, Belmaker EZ. Extreme hyperimmunoglobulinemia E and undue susceptibility to infection. *Pediatrics*. 1972;49(1):59–70.
26. Grimbacher B, et al. Hyper-IgE syndrome with recurrent infections--an autosomal dominant multisystem disorder. *N Engl J Med*. 1999;340(9):692–702.
27. Chandesris MO, et al. Autosomal dominant STAT3 deficiency and hyper-IgE syndrome: molecular, cellular, and clinical features from a French national survey. *Medicine (Baltimore)*. 2012;91(4):e1–19.
28. Yang XO, et al. STAT3 regulates cytokine-mediated generation of inflammatory helper T cells. *J Biol Chem*. 2007;282(13):9358–9363.
29. Durant L, et al. Diverse targets of the transcription factor STAT3 contribute to T cell pathogenicity and homeostasis. *Immunity*. 2010;32(5):605–615.
30. Milner JD, et al. Impaired T(H)17 cell differentiation in subjects with autosomal dominant hyper-IgE syndrome. *Nature*. 2008;452(7188):773–776.
31. Ma CS, et al. Deficiency of Th17 cells in hyper IgE syndrome due to mutations in STAT3. *J Exp Med*. 2008;205(7):1551–1557.
32. Conti HR, et al. New mechanism of oral immunity to mucosal candidiasis in hyper-IgE syndrome. *Mucosal Immunol*. 2011;4(4):448–455.
33. Kumar P, et al. Intestinal Interleukin-17 Receptor Signaling Mediates Reciprocal Control of the Gut Microbiota and Autoimmune Inflammation. *Immunity*. 2016;44(3):659–671.
34. Conti HR, et al. IL-17 Receptor Signaling in Oral Epithelial Cells Is Critical for Protection against Oropharyngeal Candidiasis. *Cell Host Microbe*. 2016;20(5):606–617.
35. Oh J, et al. The altered landscape of the human skin microbiome in patients with primary immunodeficiencies. *Genome Res*. 2013;23(12):2103–2114.
36. Smeekens SP, et al. Skin microbiome imbalance in patients with STAT1/STAT3 defects impairs innate host defense responses. *J Innate Immun*. 2014;6(3):253–262.
37. Sobel JD. Vulvovaginal candidosis. *Lancet*. 2007;369(9577):1961–1971.
38. Fidel PL. Distinct protective host defenses against oral and vaginal candidiasis. *Med Mycol*. 2002;40(4):359–375.
39. Barchiesi F, Morbiducci V, Ancarani F, Scalise G. Emergence of oropharyngeal candidiasis caused by non-albicans species of Candida in HIV-infected patients. *Eur J Epidemiol*. 1993;9(4):455–456.
40. Diaz PI, Hong BY, Dupuy AK, Strausbaugh LD. Mining the oral mycobiome: Methods, components, and meaning. *Virulence*. 2017;8(3):313–323.
41. Ghannoum MA, et al. Characterization of the oral fungal microbiome (mycobiome) in healthy individuals. *PLoS Pathog*. 2010;6(1):e1000713.
42. Dupuy AK, et al. Redefining the human oral mycobiome with improved practices in amplicon-based taxonomy: discovery of Malassezia as a prominent commensal. *PLoS ONE*. 2014;9(3):e90899.
43. Mukherjee PK, et al. Oral mycobiome analysis of HIV-infected patients: identification of Pichia as an antagonist of opportunistic fungi. *PLoS Pathog*. 2014;10(3):e1003996.
44. Findley K, et al. Topographic diversity of fungal and bacterial communities in human skin. *Nature*. 2013;498(7454):367–370.
45. Kraneveld EA, et al. The relation between oral Candida load and bacterial microbiome profiles in Dutch older adults. *PLoS ONE*. 2012;7(8):e42770.
46. Bittinger K, et al. Improved characterization of medically relevant fungi in the human respiratory tract using next-generation sequencing. *Genome Biol*. 2014;15(10):487.
47. Diaz PI, et al. Synergistic interaction between Candida albicans and commensal oral streptococci in a novel in vitro mucosal model. *Infect Immun*. 2012;80(2):620–632.
48. Falsetta ML, et al. Symbiotic relationship between Streptococcus mutans and Candida albicans synergizes virulence of plaque biofilms in vivo. *Infect Immun*. 2014;82(5):1968–1981.
49. Xu H, et al. Streptococcal co-infection augments Candida pathogenicity by amplifying the mucosal inflammatory response. *Cell Microbiol*. 2014;16(2):214–231.
50. Metwalli KH, Khan SA, Krom BP, Jabra-Rizk MA. Streptococcus mutans, Candida albicans, and the human mouth: a sticky situation. *PLoS Pathog*. 2013;9(10):e1003616.
51. Klinke T, Guggenheim B, Klimm W, Thurnheer T. Dental caries in rats associated with Candida albicans. *Caries Res*. 2011;45(2):100–106.

52. Kim D, et al. Candida albicans stimulates Streptococcus mutans microcolony development via cross-kingdom biofilm-derived metabolites. *Sci Rep*. 2017;7:41332.
53. Yang XQ, Zhang Q, Lu LY, Yang R, Liu Y, Zou J. Genotypic distribution of Candida albicans in dental biofilm of Chinese children associated with severe early childhood caries. *Arch Oral Biol*. 2012;57(8):1048–1053.
54. Raja M, Hannan A, Ali K. Association of oral candidal carriage with dental caries in children. *Caries Res*. 2010;44(3):272–276.
55. Qiu R, Li W, Lin Y, Yu D, Zhao W. Genotypic diversity and cariogenicity of Candida albicans from children with early childhood caries and caries-free children. *BMC Oral Health*. 2015;15(1):144.
56. de Carvalho FG, Silva DS, Hebling J, Spolidorio LC, Spolidorio DM. Presence of mutans streptococci and Candida spp. in dental plaque/dentine of carious teeth and early childhood caries. *Arch Oral Biol*. 2006;51(11):1024–1028.
57. De-la-Torre J, et al. Caries and Candida colonisation in adult patients in Basque Country (Spain). *Mycoses*. 2016;59(4):234–240.
58. Esposito L, et al. Hyper-IgE syndrome: dental implications. *Oral Surg Oral Med Oral Pathol Oral Radiol*. 2012;114(2):147–153.
59. Raquil MA, Anceriz N, Rouleau P, Tessier PA. Blockade of antimicrobial proteins S100A8 and S100A9 inhibits phagocyte migration to the alveoli in streptococcal pneumonia. *J Immunol*. 2008;180(5):3366–3374.
60. McLachlan JL, Sloan AJ, Smith AJ, Landini G, Cooper PR. S100 and cytokine expression in caries. *Infect Immun*. 2004;72(7):4102–4108.
61. Grimbacher B, et al. Genetic linkage of hyper-IgE syndrome to chromosome 4. *Am J Hum Genet*. 1999;65(3):735–744.
62. Jo JH, et al. Diverse Human Skin Fungal Communities in Children Converge in Adulthood. *J Invest Dermatol*. 2016;136(12):2356–2363.
63. Fadrosh DW, et al. An improved dual-indexing approach for multiplexed 16S rRNA gene sequencing on the Illumina MiSeq platform. *Microbiome*. 2014;2(1):6.
64. Schloss PD, et al. Introducing mothur: open-source, platform-independent, community-supported software for describing and comparing microbial communities. *Appl Environ Microbiol*. 2009;75(23):7537–7541.
65. Kozich JJ, Westcott SL, Baxter NT, Highlander SK, Schloss PD. Development of a dual-index sequencing strategy and curation pipeline for analyzing amplicon sequence data on the MiSeq Illumina sequencing platform. *Appl Environ Microbiol*. 2013;79(17):5112–5120.
66. Edgar RC, Haas BJ, Clemente JC, Quince C, Knight R. UCHIME improves sensitivity and speed of chimera detection. *Bioinformatics*. 2011;27(16):2194–2200.
67. Chen T, Yu WH, Izard J, Baranova OV, Lakshmanan A, Dewhirst FE. The Human Oral Microbiome Database: a web accessible resource for investigating oral microbe taxonomic and genomic information. *Database (Oxford)*. 2010;2010:baq013.
68. Al-Hebshi NN, Nasher AT, Idris AM, Chen T. Robust species taxonomy assignment algorithm for 16S rRNA NGS reads: application to oral carcinoma samples. *J Oral Microbiol*. 2015;7:28934.
69. Matsen FA, Kodner RB, Armbrust EV. pplacer: linear time maximum-likelihood and Bayesian phylogenetic placement of sequences onto a fixed reference tree. *BMC Bioinformatics*. 2010;11:538.
70. Abusleme L, et al. The subgingival microbiome in health and periodontitis and its relationship with community biomass and inflammation. *ISME J*. 2013;7(5):1016–1025.
71. Willger SD, et al. Characterization and quantification of the fungal microbiome in serial samples from individuals with cystic fibrosis. *Microbiome*. 2014;2:40.
72. St Leger AJ, et al. An Ocular Commensal Protects against Corneal Infection by Driving an Interleukin-17 Response from Mucosal γδ T Cells. *Immunity*. 2017;47(1):148–158.e5.
73. Segata N, et al. Metagenomic biomarker discovery and explanation. *Genome Biol*. 2011;12(6):R60.